A Nonlinear Hybrid Model of a 4-Cylinder Engine for Idle Speed Control*

Andrea Balluchi[†] Marco Zoncu[†] Tiziano Villa[†]
Alberto L. Sangiovanni–Vincentelli[†¶]

[†] PARADES, Via di S.Pantaleo, 66, 00186 Roma, Italy.
{balluchi, mzoncu, villa, alberto}@parades.rm.cnr.it
[¶] Dept. of Electrical Engineering and Computer Sciences,
Univ. of California at Berkeley, CA 94720, USA.

June 20, 2003

Abstract

The present document describes the second version of the *Idle Speed Control* case study, developed by PARADES within the "Computation and Control" European Project during year 2002. In the first version of the case study, a linear hybrid model of a 4-cylinder in-line engine was presented and its open-loop behavior was illustrated by some simulation results. In this document, such model has been refined by taking into account nonlinearities in the intake manifold and by modeling more precisely both the torque generation mechanism and the effect of clutch switching on the power-train dynamics. Furthermore, in order to provide a certain degree of scalability to the test case, a number of hybrid engine models at increasing levels of complexity have been illustrated, starting from a very abstract one and ending with the complex nonlinear hybrid model. Finally, simulation results of the proposed models are presented to highlight the peculiarities of each hybrid description of the engine with respect to the others.

1 Introduction

The synthesis of a control strategy for an internal combustion engine in the idle regime is one of the most challenging problems in engine control. The goal is to maintain the engine speed as close as possible to a reference constant engine speed despite load torque disturbances (i.e. the air conditioning system, the steering wheel servo-mechanism) and engagements and

*This research has been sponsored by European Community Projects IST-2001-33520 CC (Control and Computation)

disengagements of the trasmission occurring when the driver operates on the clutch. In order to achieve the best fuel economy, the reference engine speed is chosen at the minimum value that yields acceptable combustion and emission quality, and noise, vibration and harshness (NVH) characteristics. For indirect injection engines, assuming a stoichiometric air-to-fuel ratio, stability of the engine speed is achieved by controlling the amount of air supplied to the engine and the spark ignition times. In modern cars, the amount of air is controlled by directly acting on the throttle via a DC or a stepper motor(electronic throttle control). This control can provide large control authority but it is relatively slow since it is subject to the dynamics of the cylinders filling and the delay due to the mix compression. On the contrary, spark control is much faster and is actuated by anticipating/retarding the spark ignition with respect to a nominal retard from the maximum spark-to-torque efficiency value. Hence, sudden loads can be much better compensated with spark ignition than with air inflow, while air inflow can be used to control the engine in steady state. However, spark control has a limited authority since combustion inefficiency and catalyst overheating must be avoided.

In order to design a controller able to reduce substantially emission and gas consumption while maintaining idle regime stability, an accurate cycle-to-cycle model of a four–stroke gasoline engine is here proposed. The model has a "natural" hybrid representation because (*i*) pistons have four modes of operation corresponding to the stroke they are in, and (*ii*) power–train and air dynamics are continuous–time processes.

In addition, these processes interact tightly: in fact, the timing of the transitions between two phases of the pistons is determined by the continuous motion of the power–train, which, in turn, depends on the torque produced by each piston. The adoption of a hybrid formalism allows to describe the cyclic behavior of the engine, thus capturing the effect of each spark ignition on the generated torque, the interaction between the discrete torque generation and the continuous power-train and air dynamics, and the discrete changes in the power-train. The torque that is generated by each piston and applied to the engine crankshaft can be assumed to be a function of the spark ignition time, and of the air-fuel mixture mass loaded in the cylinder during the intake phase so that it can be modified by appropriately acting on the throttle valve and on the spark ignition times. Hence, the outputs of the hybrid controller are the throttle angle (continuous-time variable) and the spark ignition times for the four spark plugs (discrete-time variables).

2 Hybrid model of the engine

In this section, a hybrid system that describes the behavior of an automotive 4-cylinder engine in idle is illustrated. Figure 1 shows the interactions

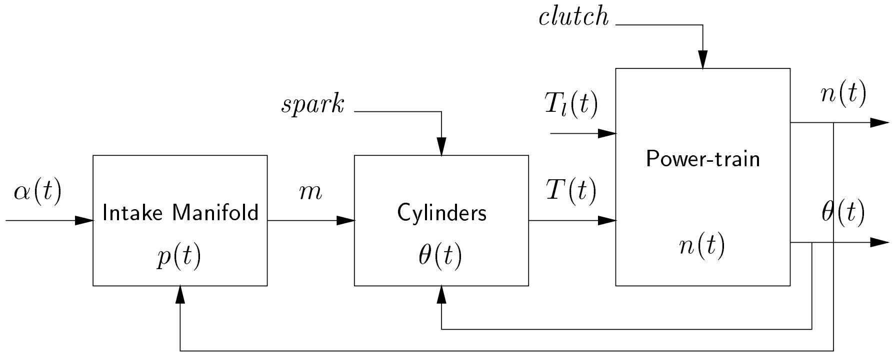

Figure 1: The engine blocks.

between the three main subsystems which compose the engine: the intake manifold, the cylinders and the power–train.
The pressure p of the intake manifold depends on the throttle valve angle α and on the crankshaft revolution speed n. The manifold pressure determines the mass of air-fuel mixture m loaded by the cylinders. In each stroke of the 4–stroke engine cycle, the cylinders evolution is described in terms of the crankshaft angle $\theta \in [0, 180]$, which defines the location of the piston within the given stroke. The torque T generated by the cylinders depends on both the mass m and the spark ignition time. Finally, the power-train dynamics, controlled by the generated torque T, is subject to the sum of load torques T_l and depends on the position of the clutch. The gear is supposed to be in idle position.

The hybrid model of the engine in idle is characterized by a set of discrete modes (corresponding to the FSM states), a set of continuous variables (subject to a continuous–time dynamics, CTS) and a set of symbolic constants (whose discrete–time evolution is described by a DES).
The control inputs are: the throttle angle α and the spark command *spk* (which can be applied from 20^0 before the end of the compression stroke to 15^0 after the beginning of the expansion stroke).
The disturbance inputs are: the load torque T_l (assumed to be nonegative and upper bounded by some T_l^M) and the *clutch*.
Hence, the controller and the environment act on the system with two kinds of inputs: the continuous inputs, α and T_l, affect the continuous dynamics; the discrete inputs, *spark* and *clutch*, determine the discrete mode transitions, the resetting of continuous variables and the setting of symbolic constants.

The engine FSM has six modes S_-, S, S_+, S_-^L, S^L, and S_+^L, see Figure 2. The three modes S_-, S, and S_+ are used to describe the interleaving between spark ignitions and dead–centers (that are reached when the pistons are at their uppermost/lowermost position) in the cylinders evolution and are related to the clutch in open position. Modes S_-^L, S^L, and S_+^L are the

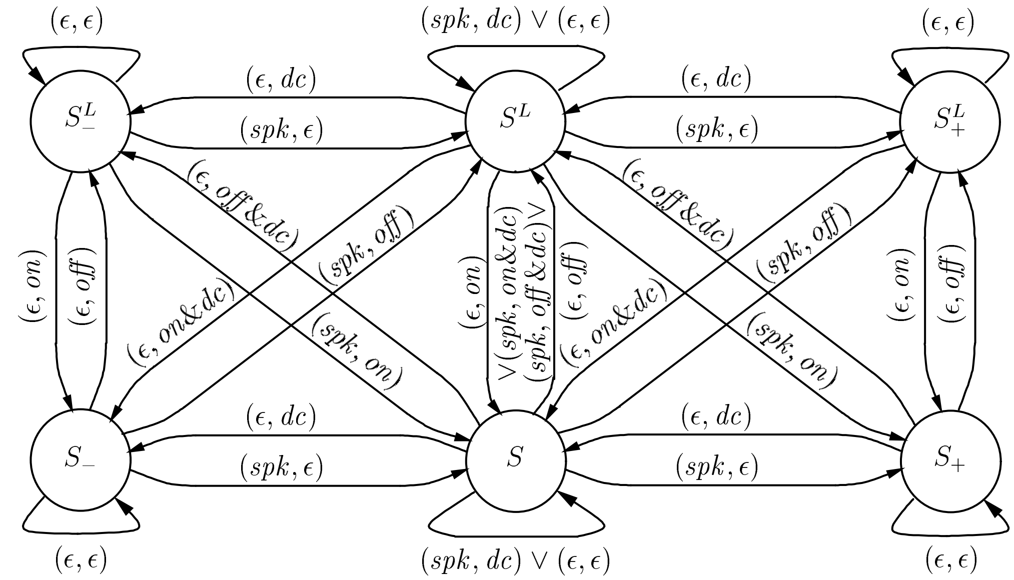

Figure 2: Engine FSM.

corresponding modes with clutch closed.

The DES has a 5–dimensional state, whose components $(T_C, T_E, m_C, m_E, \varphi)$ stand, respectively, for the torque absorbed by the cylinder in the compression stroke, the torque generated by the cylinder in the expansion stroke, the mass of mixture loaded in the cylinder in the compression stroke, the mass of mixture loaded in the cylinder in the expansion stroke and the applied spark advance. The torque T that acts on the power-train is obtained as

$$T = T_E - T_C \tag{1}$$

When the clutch is open, the CTS has a 4–dimensional state, comprehending the manifold pressure p, the crankshaft revolution speed n, the revolution speed n_g of the segment of the driveline from the clutch to the gear, and the piston position θ. When the clutch is closed, by virtue of the condition $n_g = n$, the CTS state is reduced to (p, n, θ).

The intake manifold is subject to the following dynamics:

$$\dot{p}(t) = a_p f_{out}(p(t), n(t)) + b_p S(\alpha(t)) \tag{2}$$

where

$$f_{out}(p(t), n(t)) = (G_{np} n(t) + O_{np}) p(t) + G_{nn} n(t) + O_{nn} \tag{3}$$

represents the air flow rate, and

$$S(\alpha) = a_s \alpha^2 + b_s \alpha + c_s \tag{4}$$

stands for the equivalent throttle area. The amount of air mass loaded during an intake stroke is given by:

$$f_m(p(t), n(t)) = \frac{30}{n} f_{out}(p(t), n(t)) \tag{5}$$

When the clutch is in the *open* position the two segments of the driveline are disconnected, and the power-train dynamics is given by:

$$\begin{aligned} \dot{n}(t) &= a_n^o n(t) + b_n^o (T_g(t) - T_l(t)) && (6) \\ \dot{n_g}(t) &= a_{n_g} n_g(t) && (7) \\ \dot{\theta}(t) &= k_c n(t) && (8) \end{aligned}$$

When the clutch is in the *close* position, the two segments of the driveline are connected, and the power-train dynamics is:

$$\dot{n}(t) = a_n^c n(t) + b_n^c (T_g(t) - T_l(t)) \tag{9}$$

In the equations (6) and (9), $T_g(t) = T(t) - T_p(t)$ represents the effective torque generated by the engine, while $T_p(t)$ stands for the loss of generated torque due both to pumping and friction. The dynamic parameters involved in the revolution speed equations are $a_n^o = -B/J_o$, $b_n^o = 1/J_o$, $a_{n_g} = -B/(J_c - J_o)$, $a_n^c = -B/J_c$, $b_n^c = 1/J_c$, with J_0 (J_c) and B denoting the inertial momentum and the viscous friction coefficient of the segment of the power-train from the crankshaft to the clutch (from the crankshaft to the gear, respectively).
When the driver releases the clutch pedal, the crankshaft revolution speed is reset as follows:

$$n := \frac{J_o n + (J_c - J_o) n_g}{J_c} \tag{10}$$

according to the conservation of the driveline's angular momentum. For the same reason, when the clutch is opened, the revolution speed of the driveline's segment from the clutch to the gear takes the value of that of the crankshaft:

$$n_g := n \tag{11}$$

Formally, the overall engine hybrid model is a tuple

$$H = (\{Q, X, \Xi\}, \{\Sigma_c, U\}, \{M_c^{disc}, M_c^{cts}\}, \{\Sigma_e, D\}, \{M_e^{disc}, M_e^{cts}\}, \{f, \delta\})$$

where:

- the **state space** is composed of:
    - the finite set of FSM modes $Q = \{S_-, S, S_+, S_-^L, S^L, S_+^L\}$;
    - the space of CTS variables $X = \{(p, n, n_g, \theta) \mid (p, n, n_g, \theta) \in \mathbb{R}^4\}$;

- the space of DES variables $\Xi = \{(T_C, T_E, m_C, m_E, \varphi) \mid (T_C, T_E, m_C, m_E, \varphi) \in \mathbb{R}^4\}$.

An element (q, x, ξ) in the space $Q \times X \times \Xi$ is called a *configuration*;

- the **control inputs** $\alpha(t)$ and *spark* can be described by means of:

  - the domain of continuous input values $U = [0, \alpha^M]$;
  - the finite domain of *discrete control events* $\Sigma_c = \{spk\}$ with $\Sigma_c^\epsilon = \Sigma_c \cup \{\epsilon\}$ being the set of *discrete control moves* and the special ϵ move being the *silent* move;
  - the *discrete controller feasible move function*[2] $M_c^{disc} : Q \times X \times \Xi \to 2^{\Sigma_c^\epsilon} \setminus \{\}$ as in Table 1;
  - the *continuous controller feasible move function* $M_c^{cts} : Q \times X \times \Xi \to 2^U \setminus \{\}$ described as follows: $M_c^{cts}(q, x, \xi) = \{\alpha \mid \alpha \in [0, \alpha^M]\}$, $\forall\, (q, x, \xi)$.

- the **disturbance inputs** $T_l(t)$ and *clutch* can be described by means of:

  - the domain of *continuous disturbance values* $D = [0, T_l^M]$;
  - the finite set of *discrete disturbance events* $\Sigma_e =\{on,\ off,\ dc,\ on\&dc,\ off\&dc\}$ (where the events *on* and *off* represent opening and closing the clutch, the event *dc* represents reaching a dead–center when $\theta = 180$, the events *on*&*dc* and *off*&*dc* represent the simultaneous occurrence of a clutch operation and a dead–center), and $\Sigma_e^\epsilon = \Sigma_e \cup \{\epsilon\}$ is the set of *discrete disturbance moves*;
  - the *discrete disturbance move function*[3] $M_e^{disc} : Q \times X \times \Xi \to 2^{\Sigma_e^\epsilon} \setminus \{\}$ given in Table 1;
  - the *continuous disturbance feasible move function*: $M_e^{cts} : Q \times X \times \Xi \to 2^D \setminus \{\}$ described as follows: $M_e^{cts}(q, x, \xi) = \{T_l \mid T_l \in [0,\, T_{lM}]\}$, $\forall\, (q, x, \xi)$;

- the **transitions** are described by $f : Q \times X \times \Xi \times U \times D \to \mathbb{R}^n$ that models the CTS dynamics, which depends on the mode, and the *transition function* $\delta = (\delta|_Q, \delta|_X, \delta|_\Xi) : Q \times X \times \Xi \times \Sigma_c^\epsilon \times \Sigma_e^\epsilon \to 2^{Q \times X \times \Xi} \setminus \{\}$ modeling the discrete dynamics. For each $q \in Q$, $f(q, x, \xi, \alpha, T_l)$ is given by (2), (9) and (8). The transition function δ is described in Figure 2 (FSM next–state function $\delta|_Q$) and in Table 2 (CTS state reset function $\delta|_X$ and DES dynamics $\delta|_\Xi$)).

[2]Notice that $M_c^{disc}(S_-, \theta = 15) = \{spk\}$ is a discrete control move required when the spark was not given yet and must be given now, since it is the last valid ignition time instant.

[3]Notice that $M_e^{disc}(S_+, \theta = 180) = \{dc, off\&dc\}$, $M_e^{disc}(S_+, \theta = 180) = \{dc, on\&dc\}$, $M_e^{disc}(S, \theta = 180) = \{dc, off\&dc\}$ and $M_e^{disc}(S^L, \theta = 180) = \{dc, off\&dc\}$ model discrete moves forced by the continuous state.

q	θ	M_c^{disc}	q	θ	M_e^{disc}
S	$[0, 160)$	$\{\epsilon\}$	S	$[0, 180)$	$\{\epsilon, \mathit{off}\}$
	$[160, 180]$	$\{\epsilon, spk\}$		180	$\{dc, \mathit{off}\&dc\}$
S^L	$[0, 160)$	$\{\epsilon\}$	S^L	$[0, 180)$	$\{\epsilon, on\}$
	$[160, 180]$	$\{\epsilon, spk\}$		180	$\{dc, on\&dc\}$
S_+	$[0, 180]$	$\{\epsilon\}$	S_-	$[0, 15]$	$\{\epsilon, \mathit{off}\}$
S_+^L	$[0, 180]$	$\{\epsilon\}$	S_-^L	$[0, 15]$	$\{\epsilon, on\}$
S_-	$[0, 15)$	$\{\epsilon, spk\}$	S_+	$[0, 180)$	$\{\epsilon, \mathit{off}\}$
	15	$\{spk\}$		180	$\{dc, \mathit{off}\&dc\}$
S_-^L	$[0, 15)$	$\{\epsilon, spk\}$	S_+^L	$[0, 180)$	$\{\epsilon, on\}$
	15	$\{spk\}$		180	$\{dc, on\&dc\}$

Table 1: Discrete move functions M_c^{disc} and M_e^{disc}.

q	$(spk, clutch)$	$\delta\vert_X$	$\delta\vert_\Xi$
S	(ϵ, off)	$n := \frac{(J_o n + (J_c - J_o) n_g)}{J_c}$	
	(ϵ, dc)	$\theta := 0$	$m_E := m_C,\ m_C := f_m(p,n),\ T_E := 0;$ $T_C := G^c f_m(p,n) + T_0^c$
	$(\epsilon, \mathit{off}\&dc)$	$\theta := 0$ $n := \frac{(J_o n + (J_c - J_o) n_g)}{J_c}$	
	(spk, ϵ)		$\varphi := 180 - \theta$
	(spk, off)	$n := \frac{(J_o n + (J_c - J_o) n_g)}{J_c}$	
	(spk, dc)	$\theta := 0$	$m_C := f_m(p,n),\ T_E := (G^e m_C + T_0^e)\eta(0);$ $T_C := G^c f_m(p,n) + T_0^c$
	$(spk, \mathit{off}\&dc)$	$\theta := 0$ $n := \frac{(J_o n + (J_c - J_o) n_g)}{J_c}$	
S^L	(ϵ, on)	$n_g := n$	
	(ϵ, dc)	$\theta := 0$	$m_E := m_C,\ m_C := f_m(p,n),\ T_E := 0;$ $T_C := G^c f_m(p,n) + T_0^c$
	$(\epsilon, on\&dc)$	$\theta := 0$ $n_g := n$	
	(spk, ϵ)		$\varphi := 180 - \theta$
	(spk, on)	$n_g := n$	
	(spk, dc)	$\theta := 0$	$m_C := f_m(p,n),\ T_E := (G^e m_C + T_0^e)\eta(0);$ $T_C := G^c f_m(p,n) + T_0^c$
	$(spk, on\&dc)$	$\theta := 0$ $n_g := n$	
S_-	(ϵ, off)	$n := \frac{(J_o n + (J_c - J_o) n_g)}{J_c}$	
	(spk, ϵ)		$T_E := (G^e m_E + T_0^e)\eta(-\theta);$ $T_C := G^c m_C + T_0^c$
	(spk, off)	$n := \frac{(J_o n + (J_c - J_o) n_g)}{J_c}$	
S_-^L	(ϵ, on)	$n_g := n$	
	(spk, ϵ)		$T_E := (G^e m_E + T_0^e)\eta(-\theta);$ $T_C := G^c m_C + T_0^c$
	(spk, on)	$n_g := n$	
S_+	(ϵ, off)	$n := \frac{(J_o n + (J_c - J_o) n_g)}{J_c}$	
	(ϵ, dc)	$\theta := 0$	$m_C := f_m(p,n),\ T_E := (G^e m_C + T_0^e)\eta(\varphi);$ $T_C := G^c f_m(p,n) + T_0^c$
	$(\epsilon, \mathit{off}\&dc)$	$\theta := 0$ $n := \frac{(J_o n + (J_c - J_o) n_g)}{J_c}$	
S_+^L	(ϵ, on)	$n_g := n$	
	(ϵ, dc)	$\theta := 0$	$m_C := f_m(p,n),\ T_E := (G^e m_C + T_0^e)\eta(\varphi);$ $T_C := G^c f_m(p,n) + T_0^c$
	$(\epsilon, on\&dc)$	$\theta := 0$ $n_g := n$	

Table 2: Transition functions $\delta|_X$ and $\delta|_\Xi$.

Crankshaft angle gain	k_c	$180/\pi\ deg\ s\ rad^{-1}$
Crankshaft momentum of inertia (clutch open)	J_0	$0.9\ Kg\ m^2$
Crankshaft momentum of inertia (clutch closed)	J_c	$1.04\ Kg\ m^2$
Crankshaft viscosity coefficient	B	$0.02\ Kg\ m^2\ s$
Pumping and friction torque	T_p	$20\ Nm$
Expansion torque gain	G^e	$520000\ Nm\ Kg^{-1}$
Expansion torque offset	T_0^e	$-18.93\ Nm$
Compression torque gain	G^c	$130000\ Nm\ Kg^{-1}$
Compression torque offset	T_0^c	$-4.7325\ Nm$
Spark efficiency function	$\eta(\phi)$	$\eta = 0.73 + \sqrt{0.083 + 0.005\phi}$
Manifold dynamic parameters	a_p	$-1.93510^7\ Pa\ Kg^{-1}$
	b_p	$4.51510^9\ Pa\ s^{-1}\ m^{-2}$
Air flow rate generation parameters	O_{nn}	$5.5510^{-4}\ Kg\ s^{-1}$
	G_{nn}	$-1.3910^{-6}\ Kg\ s^{-1}\ RPM^{-1}$
	O_{np}	$-7.7810^{-9}\ Kg\ s^{-1}\ Pa^{-1}$
	G_{np}	$1.5010^{-10}\ Kg\ s^{-1}\ Pa^{-1}\ RPM^{-1}$
Throttle angle/surface conversion parameters	a_s	$1.8710^{-7}\ m^2\ deg^{-2}$
	b_s	$1.9210^{-7}\ m^2\ deg^{-1}$
	c_s	$6.14310^{-6}\ m^2$

Table 3: Parameters of the engine's nonlinear model.

Manifold pressure	p	$24768\ Pa$
Torque	T	$21.34\ Nm$
Compression mass	m_c	$0.9\ 10^{-4}\ Kg$
Expansion mass	m_e	$0\ Kg$
Spark advance	ϕ	20^0
Crankshaft speed	n	$800\ RPM$
Throttle angle	α	4.29^0
Spark advance	φ	20^0

Table 4: Set-point values of state and input variables.

3 The idle-speed control problem

The goal of an idle speed controller is to keep the crankshaft revolution speed within a specified range around a reference value.
The idle speed control problem can be stated as a safety one, within the Maximal Safe Set's theoretical setting. Given a subset G_0 of the state space, composed by all the acceptable configurations according to a prescribed criterion, the Maximal Safe Set is defined as the largest subset S_0 of G_0 for which there always exists a control law that, starting from a state in S_0, is able to keep the system's trajectory within G_0 indefinitely and in spite of any possible action of the disturbance.
In our case, the set G_0 is represented by a specified range $[n_0 - \Delta, n_0 + \Delta]$ for the evolution of the crankshaft revolution speed, around the desired value n_0. A design procedure for a closed-loop controller based on the Maximal Safe Set technique is exposed in detail in [2] and [5].

4 Simulations of the nonlinear hybrid model

In this section we provide some numerical simulations of the nonlinear hybrid automaton previously described. We assume that the clutch pedal, initially pressed, be released at the instant $t = 5\ s$. In Figure 4 the evolution of the expansion torque (green) and of the compression torque (red) are showed. The evolution of the mass of air loaded in the cylinders is depicted in Figure 5. The effect of closing the clutch on the revolution speeds n and n_g of the two driveline's segments is showed respectively in Figures 6 and 7.

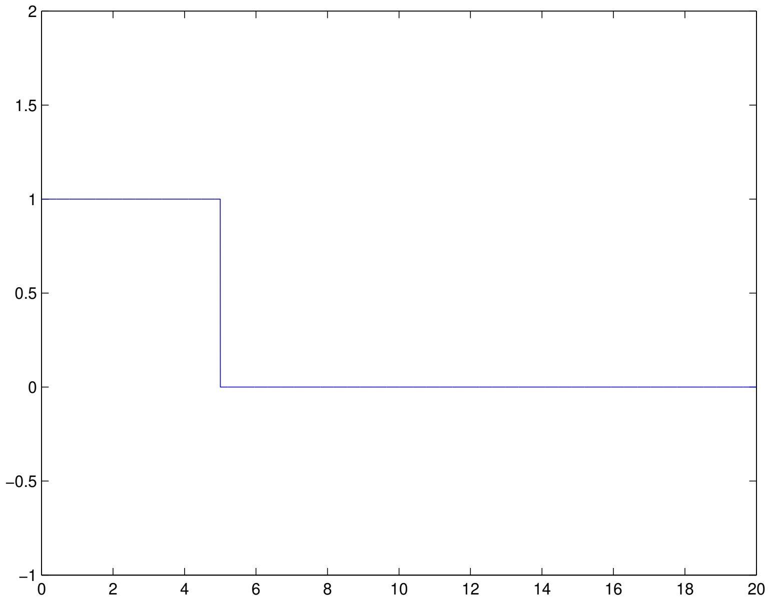

Figure 3: State of the clutch.

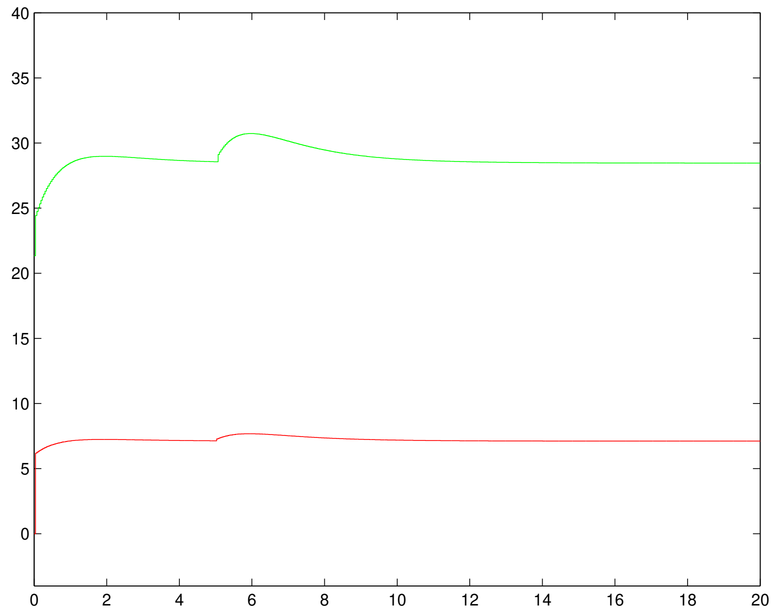

Figure 4: Compression and expansion torques in Nm.

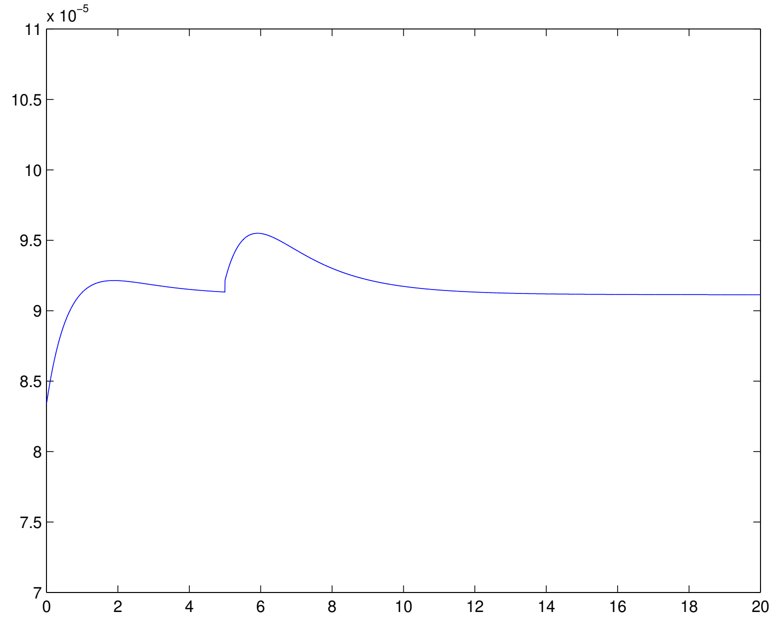

Figure 5: Mass of air loaded in Kg.

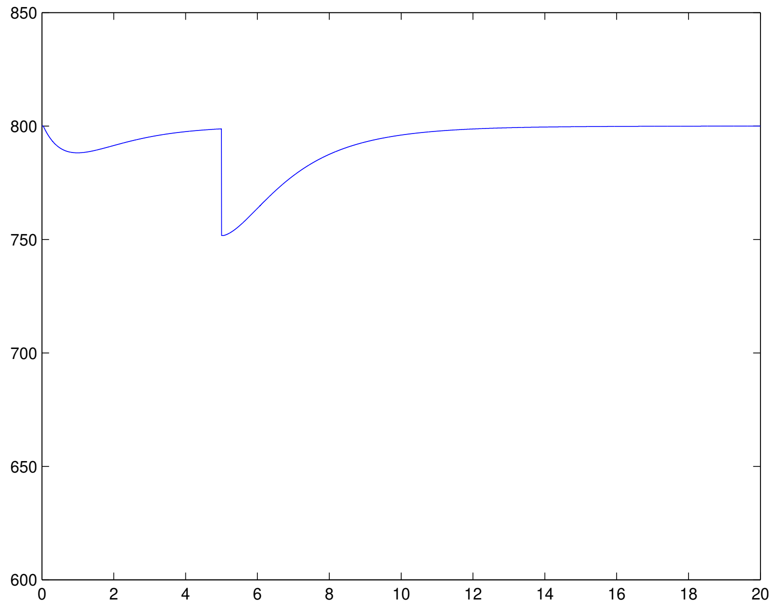

Figure 6: Crankshaft revolution speed in RPM.

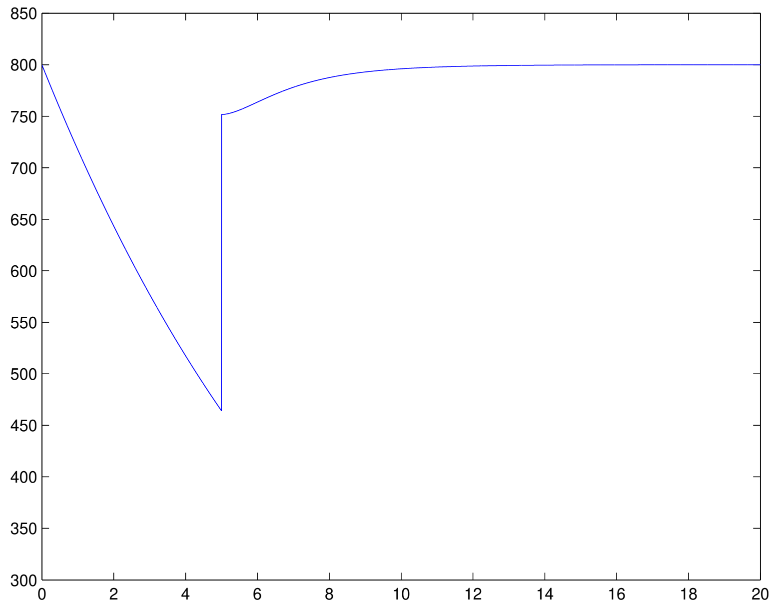

Figure 7: Revolution speed of the second driveline's segment in RPM.

5 Successive refinements of the engine's model

In this section, in order to supply better scalability to the test-case presented, we provide several hybrid representations for the 4-cylinder in-line engine in idle regime. Starting from a very simple hybrid model with a single-state FSM, successive refinements are made, up to the nonlinear hybrid model described in Section 2.

5.1 Single-location hybrid automaton

The simplest representation considered is the one depicted in Figure 8; in this case, neither the spark advance nor the manifold dynamics are modeled. Consequently, the torque is considered as an external input, belonging to the class of bounded piecewise-constant signals, assuming values in the interval $[0.6\ T_M, T_M]$, and with discontinuities synchronized with top dead centers (internal events dc). The torque value T_M stands for the maximum value of the generated torque with respect to the manifold dynamics at set point.

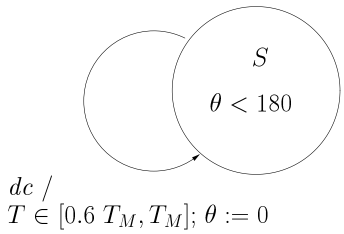

Figure 8: Single-location hybrid automaton.

The power-train's linear continuous-time dynamics is given by:

$$\begin{aligned} \dot{n}(t) &= a_n n(t) + b_n (T_g(t) - T_l(t)) \\ \dot{\theta}(t) &= k_c n(t) \end{aligned}$$

where $a_n = -B/J_o$, $b_n = 1/J_o$ (see Table 3) and $T_l \in [0, T_l^{max}]$.

5.2 Two-location hybrid automaton with spark advance

Here we consider a slightly more complex hybrid automaton, still without manifold dynamics, but with a two locations FSM, in order to model the positive spark advance ϕ; the external input event *spk* is then introduced. The hybrid automaton with positive spark advance is depicted in Figure 9.

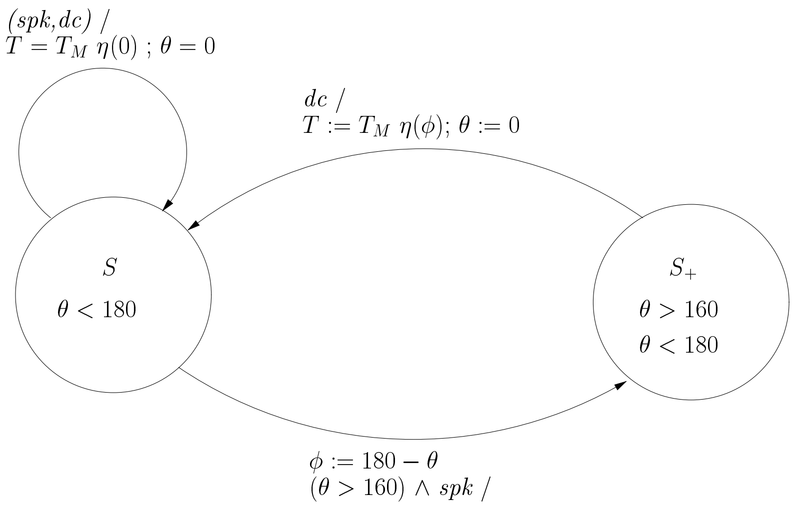

Figure 9: Two-locations hybrid automaton with spark advance.

The torque is generated, in corrispondence of each transition from S_+ to S, according to the following expression:

$$T = T_M \eta(\phi)$$

The power-train's dynamics is given by:

$$\begin{aligned} \dot{n}(t) &= a_n n(t) + b_n(T_g(t) - T_l(t)) \\ \dot{\theta}(t) &= k_c n(t) \end{aligned}$$

where $a_n = -B/J_o$, $b_n = 1/J_o$ (see Table 3) and $T_l \in [0, T_l^{max}]$.

5.3 Two-location hybrid automaton with clutch state

Let's consider another possible extension of the simple model given in Subsection 5.1: a two-location hybrid automaton is now obtained by introducing the state of the clutch, with the corresponding binary input *clutch* $\in$ {*off*, *on*} (see Figure 10). As in the model depicted in Figure 8, the torque $T \in [0.6\ T_M, T_M]$ is treated as an external input, the value of which is updated at each top dead center.

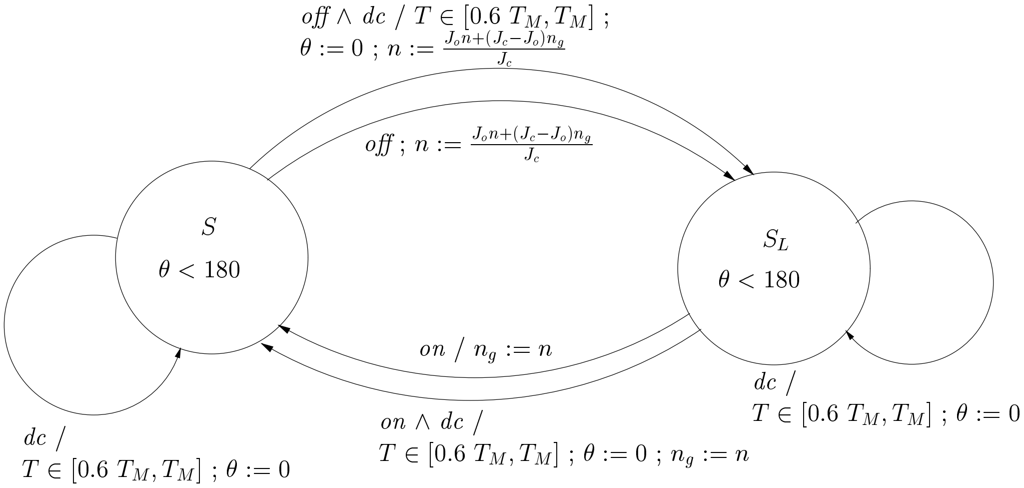

Figure 10: Two-locations automaton with clutch switching.

When the clutch is in the *open* position, the power-train dynamics is given by:

$$\dot{n}(t) = a_n n(t) + b_n(T_g(t) - T_l(t)) \tag{12}$$

$$\dot{n_g}(t) = a_{n_g} n_g(t) \tag{13}$$

$$\dot{\theta}(t) = k_c n(t) \tag{14}$$

while it is given by:

$$\dot{n}(t) = a_n n(t) + b_n(T_g(t) - T_l(t)) \tag{15}$$

when the clutch is in the *close* position.
In the equations above $a_n = -B/J_o$, $b_n = 1/J_o$, $a_{n_g} = -B/(J_c - J_o)$, $a_n = -B/J_c$ and $b_n = 1/J_c$ (see Table 3), and $T_l \in [0, T_l^{max}]$.

5.4 Two-location hybrid automaton with manifold dynamics

The two-locations hybrid automaton presented in Subsection 5.2 can be extended to take into account a linear approximation of the manifold dynamics; the automaton is depicted in Figure 11.In the hybrid model thus obtained, the torque is set at each top dead center according to the following expression:

$$T = (Gm + T_0)\eta(\phi)$$

where

$$m = G_{mp}p + M_0$$

stands for the value of the mass of mixture loaded in corrispondence of a given top dead center.

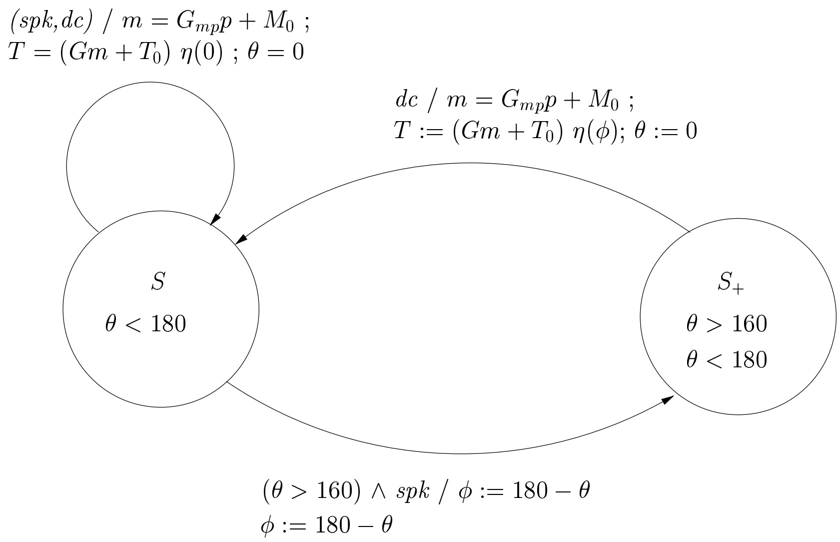

Figure 11: Two-location hybrid automaton with manifold dynamics.

The continuous-time dynamics now includes also the equation of the manifold pressure:

$$\begin{array}{rcl}\dot{p}(t) & = & a_{p_0}(p(t) - p_0) + b_{p_0}(\alpha(t) - \alpha_0) \\ \dot{n}(t) & = & a_n n(t) + b_n(T_g(t) - T_l(t)) \\ \dot{\theta}(t) & = & k_c n(t)\end{array}$$

where $a_n = -B/J_o$ and $b_n = 1/J_o$ (see Table 3), and $T_l \in [0, T_l^{max}]$. The values of the parameters a_{p_0} and b_{p_0}, as well as those of G_{mp}, M_0, G and T_0, are given in Table 5.

The quantities a_{p_0}, b_{p_0}, G_{mp} and M_0 can be obtained from the linearization of the dynamics (2) and (3) around the set point described by Table 4. The quantities G and T_0 can be obtained by averaging out the torque generation mechanism described by (1) and Table 2 over an engine's cycle. Finally, the new continuous input variable is the throttle angle α, which assumes values between 0 and α^M.

Torque gain	G	$390000\ Nm/Kg$
Torque offset	T_0	$-14.2\ Nm$
Manifold dynamic parameter	a_{p_0}	$-2.33\ s^{-1}$
Manifold dynamic parameter	b_{p_0}	$15369\ s^{-1}\ Pa\ deg^{-1}$
Pressure / mixture mass gain	G_{mp}	$4.510^{-9}\ Kg\ Pa^{-1}$
Mixture mass offset	M_0	$-2.0810^{-5}\ Kg$

Table 5: Parameters of the engine's linear model.

5.5 Three-location hybrid automaton

By adding the possibility of using negative spark advances to the model described in Subsection 5.4, the three-location hybrid model of the engine depicted in Figure 12 is obtained.
In order to deal with negative spark advances, the variables m_c (mass of air loaded in the cylinder that is in the compression stroke) and m_e (mass of air loaded in the cylinder that is in the expansion stroke) must be introduced. As shown in Figure 12, the torque generation mechanism is slightly more complex than in the previous cases. For zero or positive spark advance, the new torque value is generated in correspondence of a top dead center according to the expression:

$$T = (Gm_c + T_0)\eta(\phi)$$

with G and T_0 as in Table 5. When a negative spark advance is specified, the torque value is updated in correspondence of the *spark* event, according to the expression:

$$T = (Gm_e + T_0)\eta(-\theta)$$

At each top dead center, the compression mass m_c is updated as follows:

$$m_c = G_{mp}p + M_0$$

with G_{mp} and M_0 given in Table 5. The expansion mass m_e, when a negative spark advance is specified, simply takes the value of m_c.

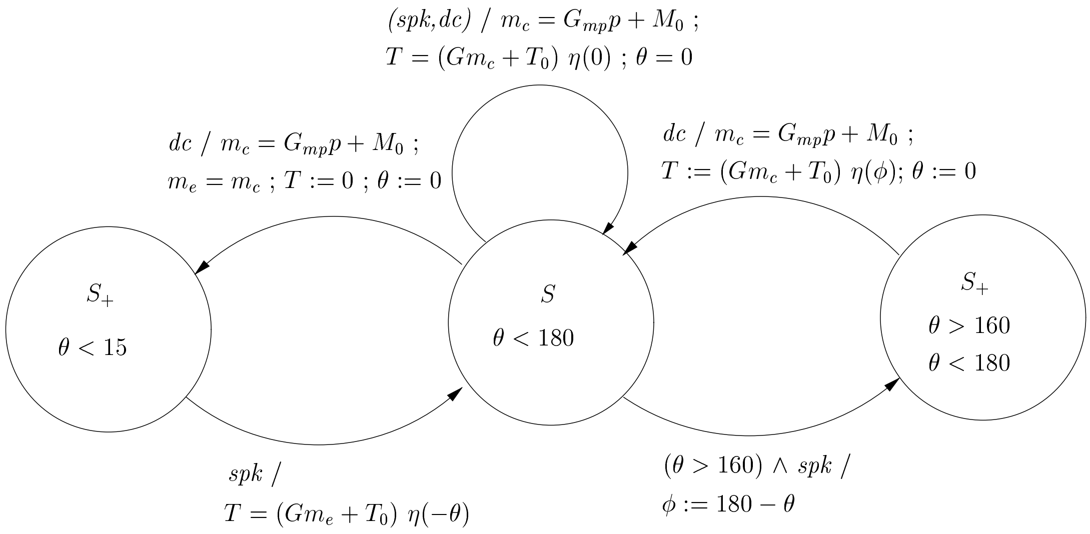

Figure 12: Three-location hybrid automaton.

Finally, the continuous-time dynamics is given by:

$$
\begin{aligned}
\dot{p}(t) &= a_{p_0}(p(t) - p_0) + b_{p_0}(\alpha(t) - \alpha_0) \\
\dot{n}(t) &= a_n n(t) + b_n(T_g(t) - T_l(t)) \\
\dot{\theta}(t) &= k_c n(t)
\end{aligned}
$$

with a_{p_0} and b_{p_0} as in Table 5, $\alpha \in [0, \alpha^M]$, $a_n = -B/J_o$ and $b_n = 1/J_o$.

5.6 Six-location hybrid automaton

The succession of engine's models of increasing complexity presented in the previous subsections can be concluded with the six-location linear hybrid automaton described in the first version of the case study [4]. It can be obtained by adding the state of the clutch to the three-location hybrid automaton described in Subsection 5.5.

6 Comparative Simulations

The hybrid models given in the previous section have been simulated open-loop under some different working conditions, in order to highlight each model's own degree of expressiveness. In each of the following subsections we propose a comparison between two different models, in which the more complex one behaves in a more realistic or efficient way than the other.
In the figures reproducing the simulation results, the generated torque and the crankshaft revolution speed are represented by blue signals, while the load torque is denoted through a red one; the green and cyan vertical lines, where present, stand respectively for dead center and spark events.

6.1 Single-location Vs Two-location with spark advance

Here we compare the behavior of the single-location hybrid automaton (Figure 8) and of the two-location one with spark advance (Figure 9), when the value of the generated torque is changed in order to compensate a sudden load reduction.
Initially, the system is in the steady state given by $n = 800\ RPM$, $T = 2.2\ Nm$, $T_l = 0.86\ Nm$ and $\phi = 20^0$. At the instant $t = 0.11\ s$, the load torque is set to zero; in correspondence of the subsequent dead center, the applied torque is consequently reduced to 1.34 Nm. In the single-location model, the torque variation manifests itself immediately (see Figure 14), and therefore the revolution speed is basically kept around 800 RPM (Fig 13).
In the two-location hybrid model, on the contrary, the new value of the spark advance $\phi = 14^0$, specified in $t = 0.11\ s$, produces the torque value $T = 1.34\ Nm$ one dead center later (see Figure 16). As a consequence, the revolution speed increases up to 800.3 RPM, thus stabilizing the system on a slightly different equilibrium point.

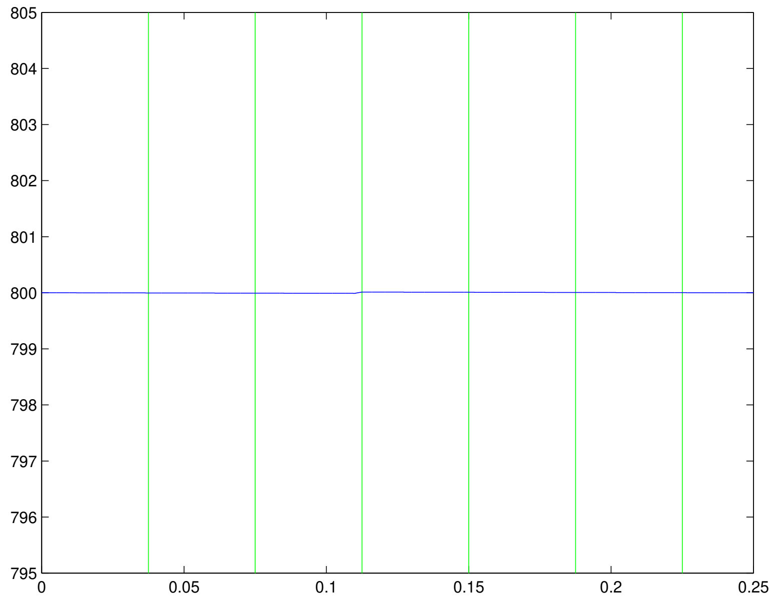

Figure 13: Single-location hybrid automaton: revolution speed.

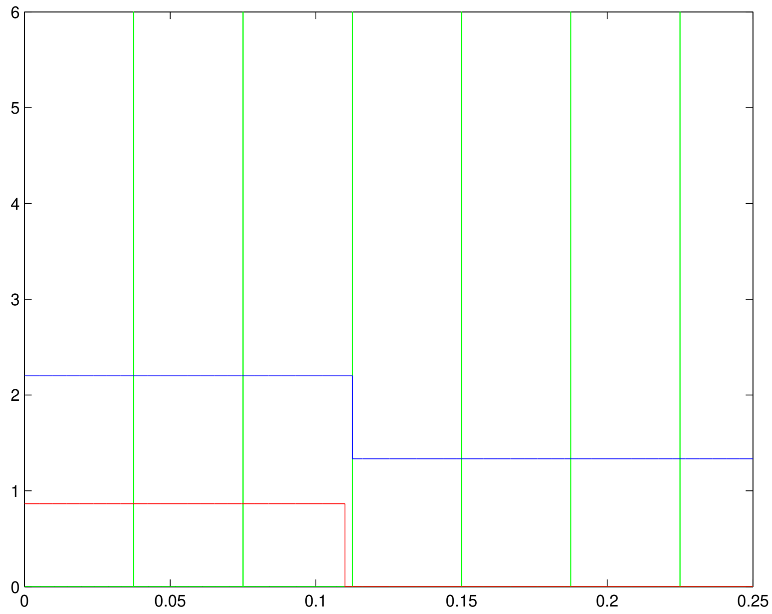

Figure 14: Single-location hybrid automaton: generated and load torques.

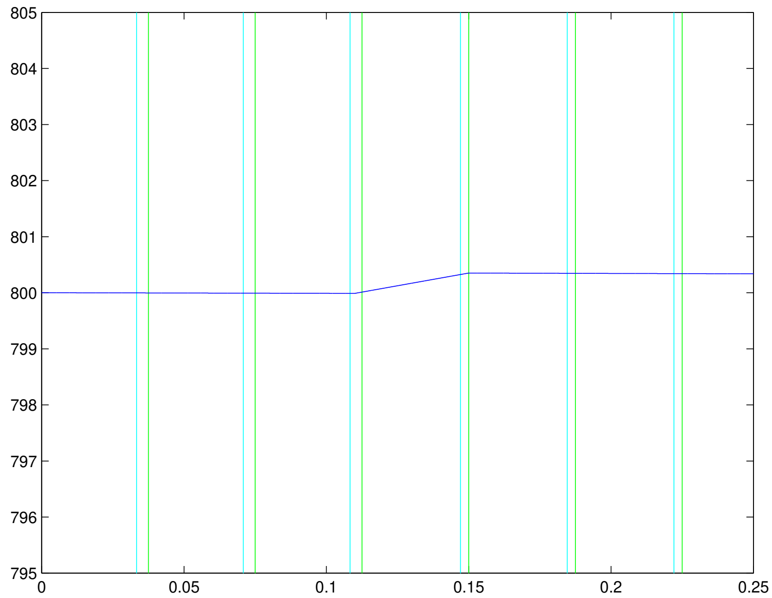

Figure 15: Two-location hybrid automaton: revolution speed.

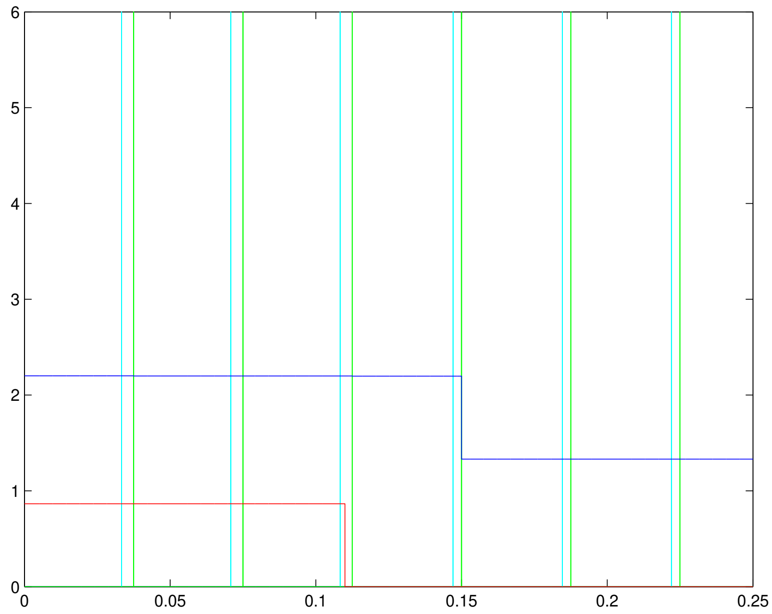

Figure 16: Two-location hybrid automaton: generated and load torques.

6.2 Two-locations with and without manifold

As already pointed out in Section 2, a control action achieved exclusively through the use of the spark advance is generally faster than one carried out by regulating only the air inflow. Nevertheless, while the former strategy has a narrow range of intervention, the latter has very large control capabilities. The first aspect will be considered in the next subsection. Here we show how the manifold-less hybrid automaton (Subsection 5.2) can not be controlled, by modulating the spark advance, to counterbalance a given increment of the load torque, while the hybrid automaton described in Subsection 5.4 can.

Initially, both the automata are in the steady state given by $n = 800\ RPM$, $T = 1.34\ Nm$, $T_l = 0$ and $\phi = 6.7^0$; for the second one we have the additional set-point values $\alpha = 3.26^0$ and $p = 26113\ Pa$. At the instant $t = 1.5$ s, the load is increased by $3\ Nm$. The spark advance of the manifold-less automaton is then set to 20^0, but the torque thus generated is not sufficient to compensate the new load torque (Figures 17 and 18). The second automaton, instead, can be brought to a new equilibrium point, characterized by $n = 794.5\ RPM$, $T = 4.34\ Nm$ and $p = 26578\ Pa$, by setting $\alpha = 3.33^0$ and $\phi = 20^0$ (see Figures 19, 20, and 21).

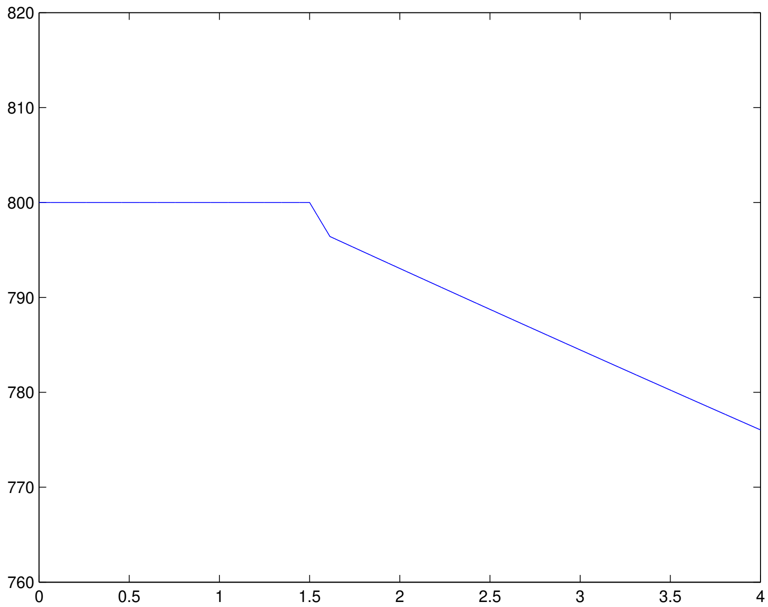

Figure 17: Two-location hybrid automaton without manifold: revolution speed.

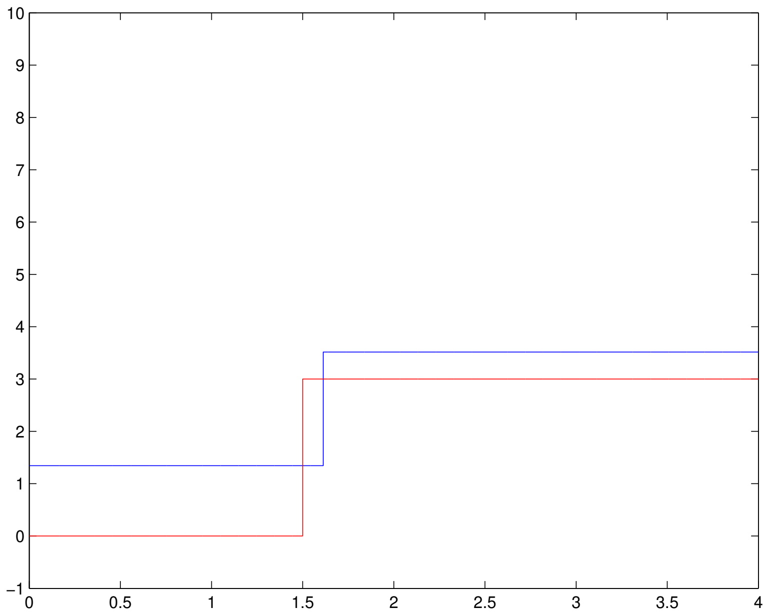

Figure 18: Two-location hybrid automaton without manifold: generated and load torques.

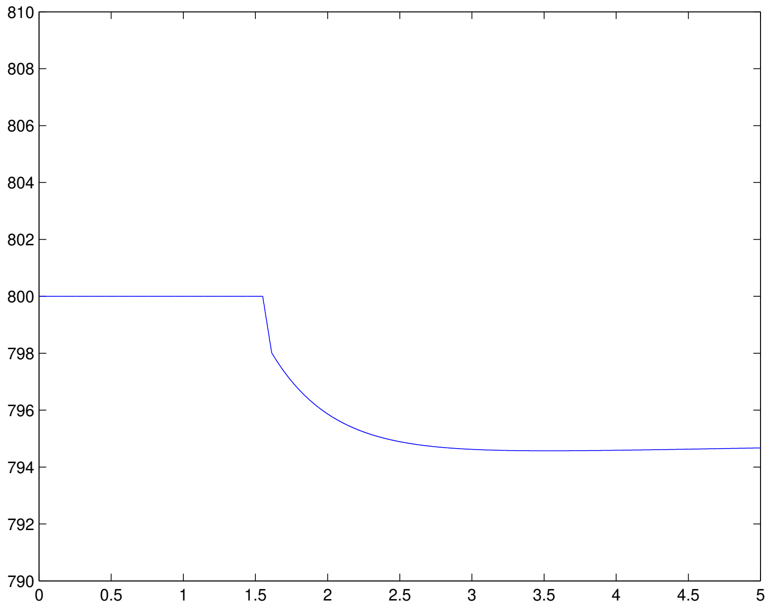

Figure 19: Two-location hybrid automaton with manifold: revolution speed.

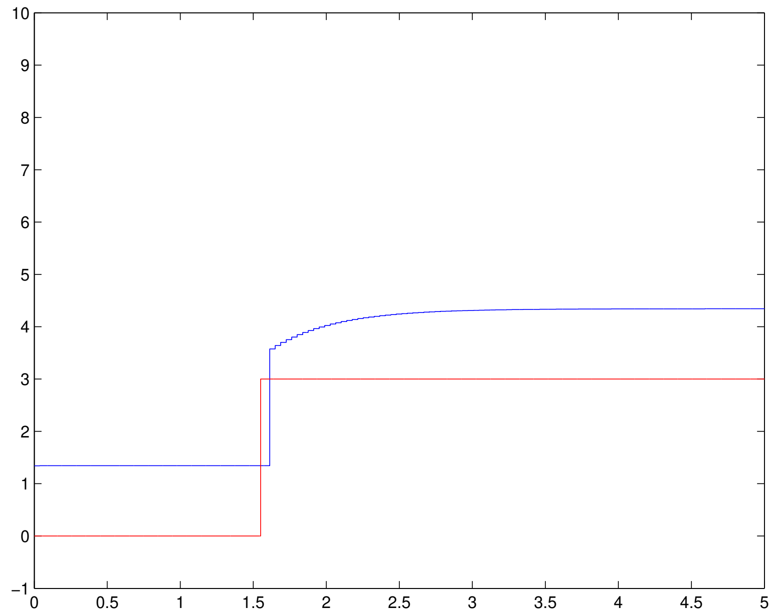

Figure 20: Two-location hybrid automaton with manifold: generated and load torques.

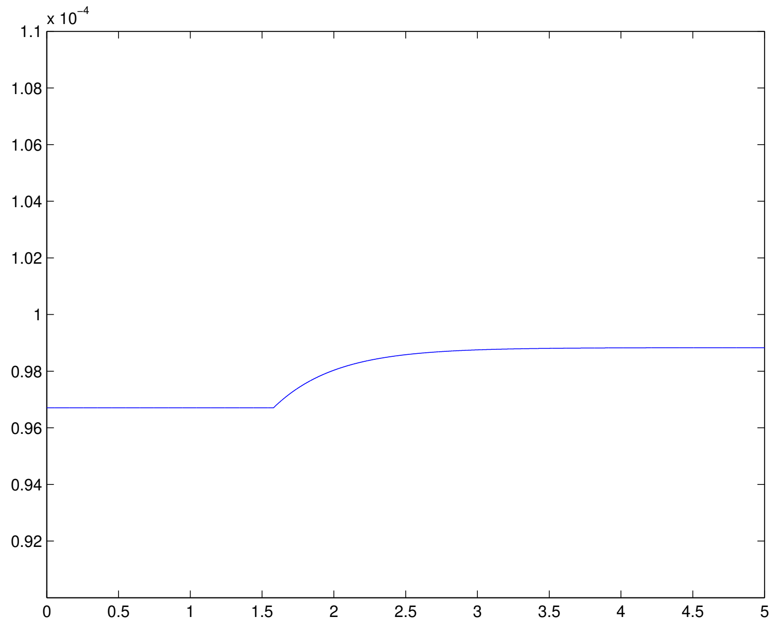

Figure 21: Two-location hybrid automaton with manifold: mass of air loaded in the cylinders.

6.3 Two-locations Vs Three-locations automata

In this subsection we compare the capabilities of the two-locations-with-manifold automaton previously described and of the three-locations automaton depicted in Figure 12, in counterbalancing a large load decrease. Initially, the automata are both in the steady state given by $p = 27985\ Pa$, $n = 800\ RPM$, $\alpha = 3.56^0$, $\phi = 5^0$, $T = 3.96\ Nm$ and $T_l = 2.62\ Nm$.
At the instant $t = 1.55\ s$, the load torque falls down to zero. In order to compensate such a decrease, the three-locations automaton is quickly driven to the new steady state characterized by $n = 800.6\ RPM$ (mean value of the saw-tooth dynamics) and $T = 1.34\ Nm$ (mean value of the square wave dynamics), by setting $\phi = -3.67^0$. For the two-locations automaton, on the contrary, it is necessary to act not only on the spark advance, that is set to zero, but also on the value of the throttle angle α, that is reduced to 3.415^0. After some seconds, the new steady state, given by $n = 808\ RPM$ and $p = 27019\ Pa$ is reached. As shown by Figures 22 and 24, the use of negative spark advance results in a much faster response.

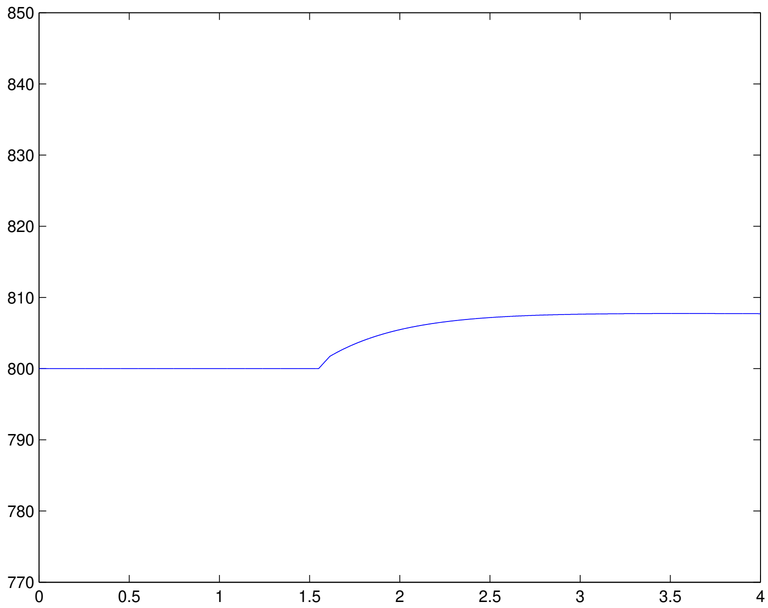

Figure 22: Two-location hybrid automaton with manifold: revolution speed.

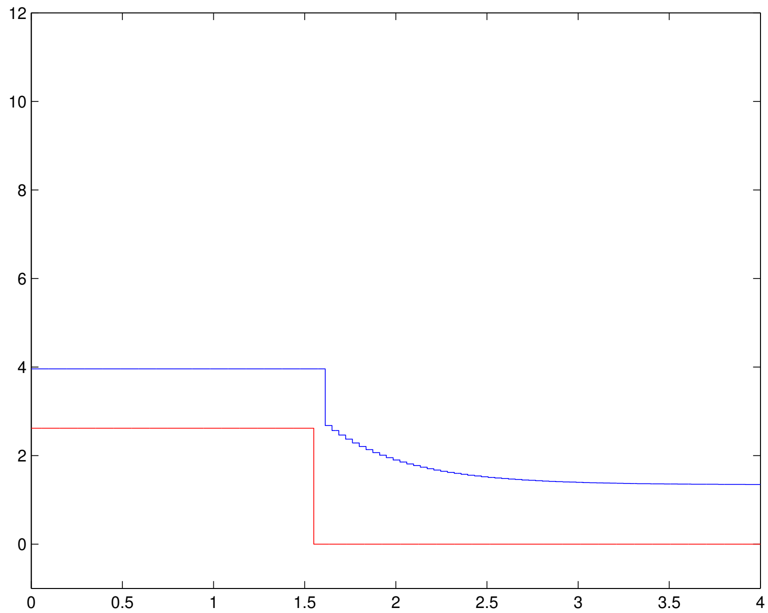

Figure 23: Two-location hybrid automaton with manifold: generated and load torques.

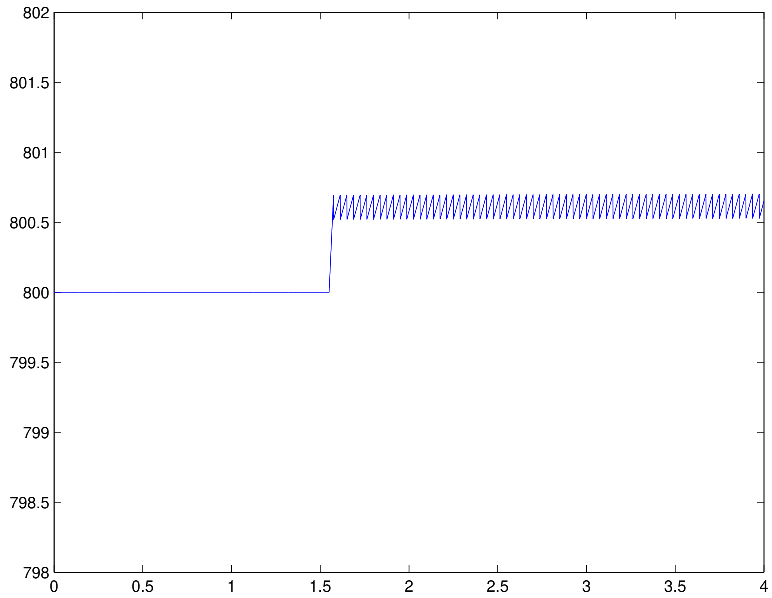

Figure 24: Three-location hybrid automaton: revolution speed.

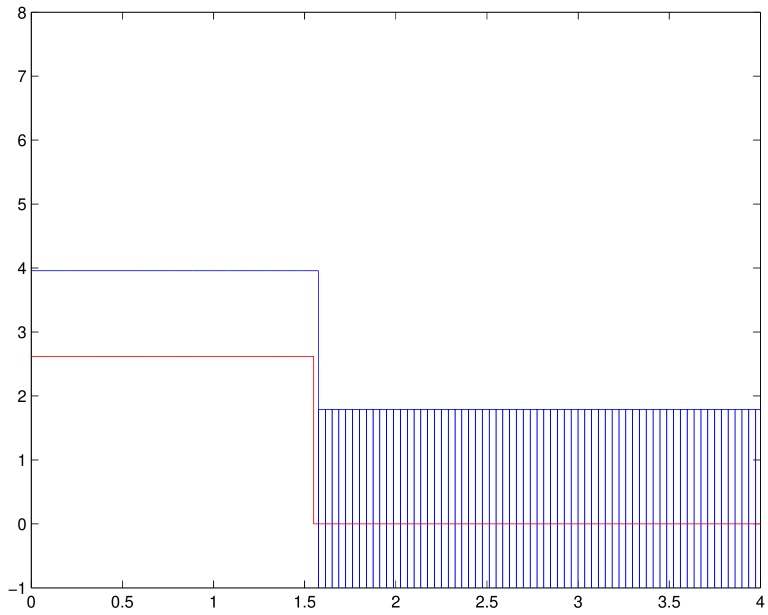

Figure 25: Three-location hybrid automaton: generated and load torques.

References

[1] A. Balluchi, L. Benvenuti, M.D. Di Benedetto, C. Pinello, and A.L. Sangiovanni–Vincentelli, "Automotive engine control and hybrid systems: Challenges and opportunities," *to appear in Proceedings of the IEEE*, 2000.

[2] A. Balluchi, L. Benvenuti, H. Wong-Toi, T. Villa, and A. L. Sangiovanni-Vincentelli, "Controller synthesis for hybrid systems with lower bounds on event separation," in *Proc. 38th IEEE Conference on Decision and Control*, Phoenix, Arizona, USA, December 1999, pp. 3984–3989.

[3] A. Balluchi, L. Benvenuti, M. D. Di Benedetto, G. M. Miconi, U. Pozzi, T. Villa, H. Wong-Toi, and A. L. Sangiovanni-Vincentelli, "Maximal safe set computation for idle speed control of an automotive engine," in *HSCC'00, Hybrid Systems: Computation and Control*.

[4] A. Balluchi, L. Benvenuti, T. Villa, A. L. Sangiovanni-Vincentelli and M. Zoncu "A Hybrid Model of a 4-Cylinder Engine for Idle Speed Control," *Test Case for the Computation and Control European Project*, March 2002.

[5] J. Lygeros, C. Tomlin and S. Sastry, "Controllers for Reachability Specifications for Hybrid Systems," in *Automatica*, March 1999, vol.35, num. 3.